Met. Mater. Int., Vol. 22, No. 5 (2016), pp. 771~780
doi: 10.1007/s12540-016-6217-0

Correlation Between Bonding Strength and Mechanical Properties in Mg/Al Two-Ply Clad Sheet

Jung-Su Kim[1], Jaeyeong Park[1], Kwang Seok Lee[2], Sunghak Lee[1], and Young Won Chang[1,*]

[1]Center for Advanced Aerospace Materials, Pohang University of Science and Technology, Pohang 37673, Korea
[2]Materials Deformation Department, Light Metal Division, Korea Institute of Materials Science, Changwon 51508, Korea

(received date: 30 March 2016 / accepted date: 17 May 2016)

The effect of interfacial bonding strength has been investigated in relation to mechanical properties of roll-bonded two-ply Mg/Al clad sheets in this study. Two types of thin reaction layers ($Mg_{17}Al_{12}$ and Mg_2Al_3 phase layers) were observed to form along the Mg/Al interface and their thickness was found to increase with annealing time. The maximum average bonding strength was achieved after annealing Mg/Al clad sheet for 10 min at 300 °C. The fracture strain of Mg alloy in this annealed clad sheet was found to increase up to 22.5% compared to 17.8% of monolithic AZ31 Mg alloy. In addition, the formability of clad Mg alloy was also found much higher compared to those of monolithic Mg alloy. This ductility enhancement of clad Mg alloy appears due to more prolonged homogeneous deformation, caused by delayed localized necking.

Keywords: Mg/Al clad sheet, microstructure, annealing, diffusion bonding, mechanical properties

I. INTRODUCTION

Multi-layered metallic clad sheets are manufactured by combining two or more alloys and have recently received significant attention for advanced structural materials in automotive, aerospace, and kitchen utensils industries, and so on. Disadvantages of monolithic alloys can effectively be improved by providing new multi-functional properties characteristic to each metallic alloy [1-4]. Various multi-layered metallic clad sheets have generally been manufactured by using Al alloys, Cu alloys, Ti alloys, carbon steels, or stainless steels to utilize their excellent properties in terms of heat conductivity, electrical conductivity and corrosion resistance as well as other specific mechanical properties [5,6].

Issues of global warming have been raised seriously all over the world, generating a number of research works focusing on new advanced lightweight materials in an attempt to reduce carbon dioxide emission. In this regard, Mg alloys have been developed as one of the promising lightest-weight metals due to their various advantageous properties in terms of specific strength, damping capacity, electromagnetic shielding, and dimensional stability [7,8]. Actual industrial applications of Mg alloys are, however, quite limited to date due to their inherent drawbacks of poor corrosion resistance, formability, and surface quality. Various types of metallic clad sheets composed of Mg alloys have thus been developed by bonding with other alloy sheets such as Al alloys or stainless steels in order to complement the inherent shortcomings of Mg alloys [9-12].

Two-ply Mg/Al clad sheets have been manufactured by utilizing various solid-state bonding processes, such as roll-bonding, friction-bonding, diffusion-bonding, and explosion-bonding [13-17]. Among these processes, roll-bonding technique has been the most widely used method due to its low production cost combined with high productivity by utilizing conventional rolling facilities as well as wide combination of clad metals [18]. As-roll-bonded Mg/Al clad sheet generally exhibits, however, typical rolling microstructure with high dislocation and twin densities, requiring post-annealing treatment in order to improve ductility through static recrystallization and grain coarsening of theses heavily deformed microstructures [19,20]. Ductility of monolithic Mg and Al alloys can be improved significantly by annealing treatment, but brittle intermetallic compound (IMC) layers are inevitably formed along the interface of Mg/Al clad sheets during annealing. Formation of these IMC layers at the interface can considerably reduce the quality of clad sheets due to the loss of interfacial bonding strength through an abrupt interfacial de-bonding.

In this study, two-ply Mg/Al clad sheets were first fabricated by a roll bonding process followed by an annealing treatment.

*Corresponding author: ywchang@postech.ac.kr

Microstructures of fabricated clad sheets were then analysed, while their mechanical properties were consequently evaluated by conducting tensile tests as well as Erichsen and roller drum peel tests. The effects of bonding strength on deformation behaviour in roll-bonded Mg/Al clad sheets have been investigated by focusing on how the thickness of interfacial IMC layers affects the mechanical properties of Mg/Al clad sheets under various loading conditions.

2. EXPERIMENTAL PROCEDURES

2.1. Two-ply Mg/Al clad sheet

A two-ply clad sheet with commercial AZ31 Mg and 1050 Al alloys were first fabricated to 3.08 mm thick sheet through multi-pass warm-rolling process at 400 °C with the reduction ratio of 23%, as schematically shown in Fig. 1. Both of the AZ31 Mg and 1050 Al alloy sheets had the initial thickness of 2.0 mm, while their nominal compositions were Mg-3.0Al-0.4Mn-0.8Zn-(≤0.1)Si and Al-(≤0.40)Fe-(≤0.25)Si-(≤0.05)Cu-(≤0.05)Mn-(≤0.05)Mg (wt%), respectively. These roll-bonded clad sheets were then annealed at 300 °C for 10, 30, and 60 min before air-cooling. As-roll-bonded clad sheet is referred to as 'AR', while the sheets annealed at 300 °C for 10, 30, and 60 min are designated as 'A1', 'A3', and 'A6', respectively as listed in Table 1.

2.2. Microstructural analysis

Clad sheets were sectioned and mechanically polished with a diamond paste with 1 μm size to observe the microstructures of longitudinal-short transverse (L-S) planes by using an optical microscope (OM, Eclipse MA200 model, NIKON, Japan). An etchant containing 10 ml acetic acid, 4.2 g picric acid, 10 ml H_2O, and 70 ml ethanol were used to etch AZ31 Mg alloy side, while an electrochemical etching was carried out for 1050 Al alloy side in a solution containing 5 ml of HBF4 and 95 ml of distilled water under the electric potential of 15 V for 90 s. Microstructural features along the interface between 1050 Al and AZ31 Mg alloys were also observed by using a scanning electron microscope (SEM, MIRA II model, TESCAN, Czech Republic) attached with an energy-dispersive X-ray spectrometer (EDS).

2.3. Tensile test

Macroscopic tensile properties were then examined using a standard ASTM E8M-01 specimen having a dog-bone-type shape with the gauge length of 25 mm, prepared along the rolling direction of two-ply clad sheets [21]. Tensile test specimens of constituent alloys were also prepared by cross-sectioning through the interface of two-ply tensile specimen using an electrical discharge machine (EDM), followed by parallel grinding. They were consequently tested at room temperature under the strain rate of 10^{-3}/s using a universal testing machine (Instron 8801 model, Canton, MA, USA) with the maximum load capacity of 100 kN.

2.4. Peel test

The average bonding strength of Mg/Al interface was measured according to the ASTM-D3167 specification [22]. Roller-drum peel tests were performed to evaluate the interfacial bonding strength using sheet-type clad specimens prepared along the longitudinal direction having the dimensions of 100 × 10 mm consisting of 0.40 mm thick Al sheet and 1.54 mm thick Mg ply. They were tested at room temperature under the cross-head speed of 6 mm/min by using the same screw-driven universal testing machine.

2.5. Erichsen test

Erichsen tests were also carried out at room temperature using graphite grease as lubricant to investigate the press formability of roll-bonded Mg-Al sheets using a hemispherical punch

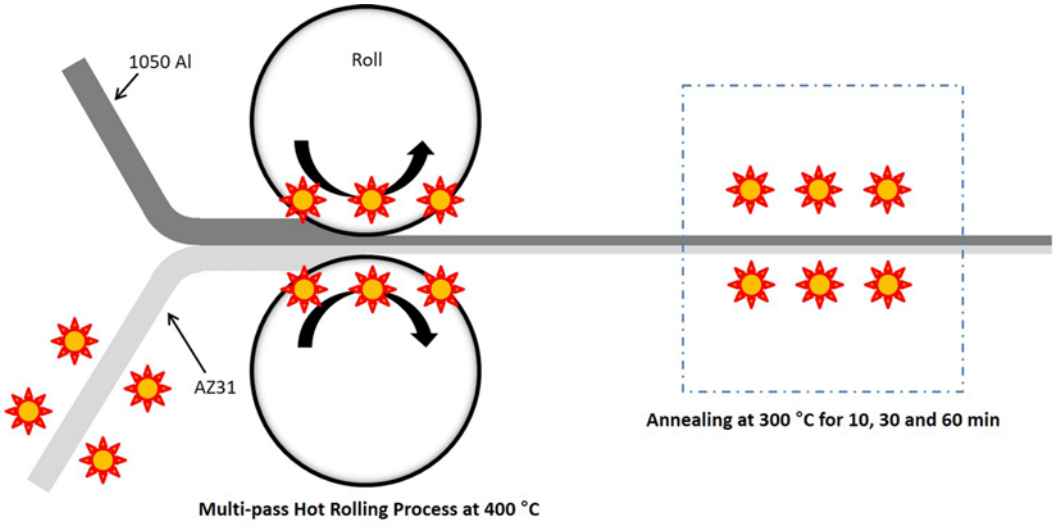

Fig. 1. Fabrication of two-ply Mg/Al clad sheet is schematically illustrated.

with the diameter of 30 mm. Circular blanks with the diameter of 50 mm were machined from Mg/Al two-ply sheets for this test. The Erichsen values (IE) were measured from these tests as the height of punch stroke at fracture initiation. Punch speed was set to 5 mm/min under the blank-holder force of 10 kN.

2.6. Digital image correlation

Strain fields in clad materials could be determined by using a digital image correlation (DIC) method, which is based on the recognition of geometrical changes in a random black-and-white speckled pattern distribution before and after straining. In this study, the evolution of equivalent strain distribution at the side surface of tensile specimens was analysed by using the ARAMIS 5M strain system during the tensile test. In order to investigate the characteristics of the interfaces between Mg and Al alloys, the horizontal strain distribution (thickness direction) at the side surface of tensile specimens was also measured. Two cameras were installed in the ARAMIS 5M strain system with the resolution of 2448 × 2050 pixels. The optimal facet and step size were found to be 15 and 10 pixels, respectively and these optimal conditions provided a spatial resolution of 60 μm for strain measurements.

3. RESULTS

3.1. Microstructural evolution of constituent alloys and Mg/Al interfaces

Microstructures of constituent AZ31 Mg alloy were observed by an optical microscope on the cross-sectional areas of AR, A1, A3, and A6 specimens and the results are shown in Figs. 2(a) through (d). AZ31 Mg alloy in AR sheet was found to consist of small grains in shear zone and coarse grains in the remaining fraction, presumably due to non-uniform deformation applied during the roll-bonding process. During the subsequent annealing process, smaller grains within heavily deformed shear zone were observed to become equi-axed resulting into a more homogeneous microstructure in terms of both the morphology and grain size as shown in Figs. 2(b) through (d). Microstructures of constituent 1050 Al alloy were also observed on the cross-sectional areas of AR, A1, A3, and A6 specimens by using an optical microscope and the results are given in Figs. 3(a) through (d). Microstructures of the 1050 Al alloys were not changed much, irrespective of annealing time.

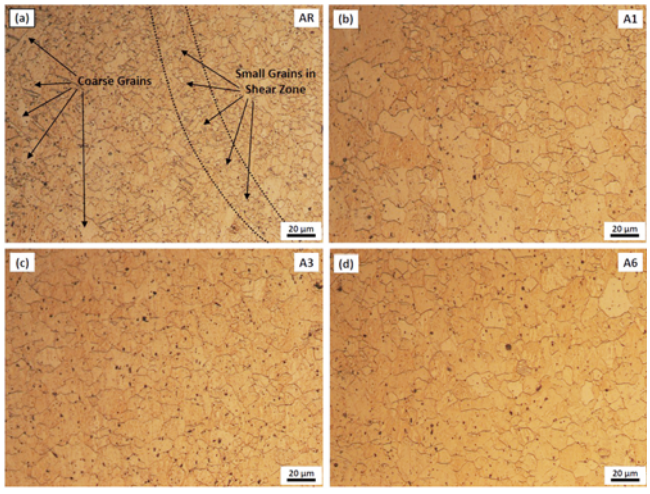

Fig. 2. Microstructures of AZ31 Mg alloy annealed for (a) 0 min, (b) 10 min, (c) 30 min, and (d) 60 min at 300 °C.

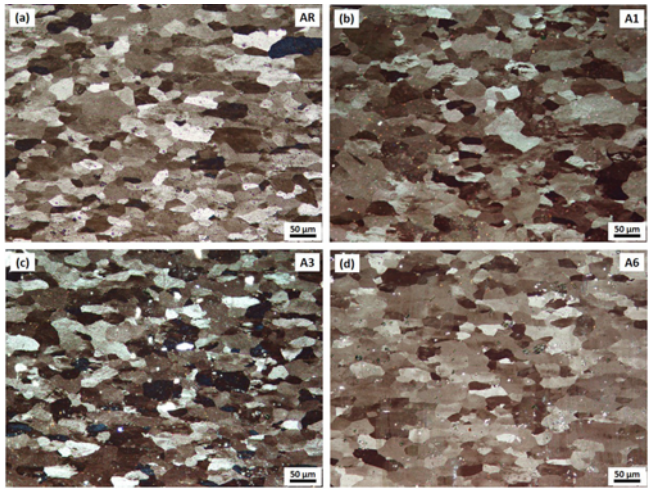

Fig. 3. Microstructures of 1050 Al alloy annealed for (a) 0 min, (b) 10 min, (c) 30 min, and (d) 60 min at 300 °C.

SEM micrographs were also observed by using a SEM on the cross-sectional areas of AR, A1, A3, and A6 specimens and the results are given in Figs. 4(a) through (d) together with the EDS composition profiles across the Mg/Al interface. These observations revealed defect-free or crack-free joining of Mg/Al interfaces both in as-roll-bonded and annealed

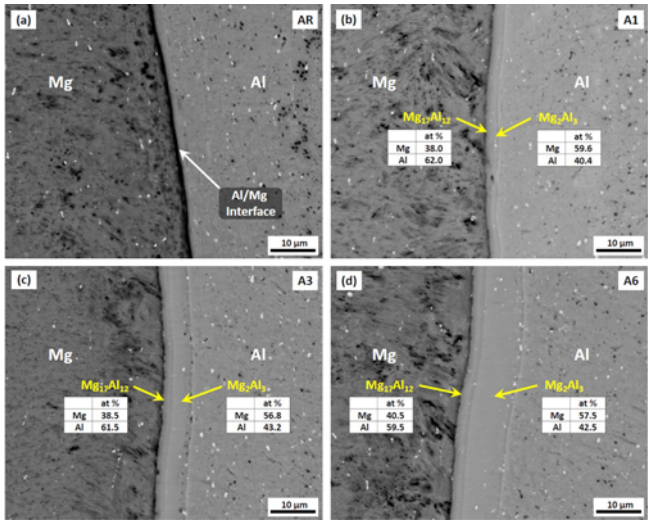

Fig. 4. SEM micrographs together with EDS analysis results at the Mg/Al interface after annealing for (a) 0 min, (b) 10 min, (c) 30 min, and (d) 60 min at 300 °C.

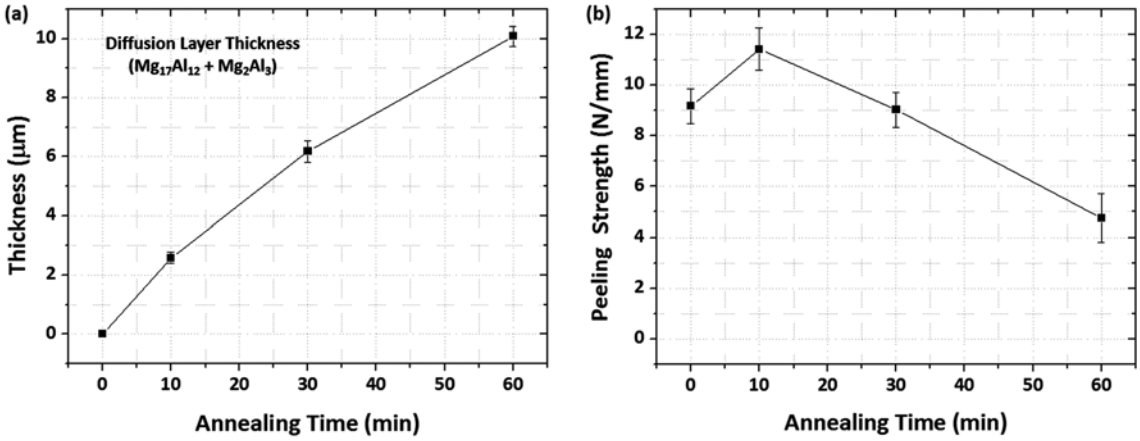

Fig. 5. (a) Thickness changes in diffusion layer (b) average bonding strength of Mg/Al interface of clad sheets are plotted in relation to annealing time.

samples. The composition profiles in the Mg/Al interface provide a clear evidence for atomic diffusion occurred during an annealing treatment at 300 °C, to form 2.6 μm, 6.2 μm, and 10.1 μm thick diffusion layers in A1, A3, and A6 specimens, respectively. Developed diffusion layers were then identified as $Mg_{17}Al_{12}$ phase adjacent to parent Mg side and Mg_2Al_3 phase adjacent to parent Al side from the Al-Mg phase diagram [23-25].

3.2. Average bonding strength of Mg/Al interface

Thickness changes in diffusion layer and average bonding strength of Mg/Al interface are plotted in terms of annealing time in Figs. 5(a) and (b), respectively. The thickness of diffusion layer can be observed to increase with annealing time, thickening up 10 μm in A6 specimen annealed for 60 min at 300 °C from Fig. 5(a). Variation of average bonding strength given in Fig. 5(b) exhibits the maximum strength of 11.4 N/mm after annealing for 10 min and then observed to decrease gradually with further annealing reaching down to 4.8 N/mm after 60 min. Average bonding strength of Mg/Al interface is now well accepted to depend strongly on the formation and growth of brittle intermetallic compound (IMC) consisting of $Mg_{17}Al_{12}$ and Mg_2Al_3 [26,27]. There have been numerous reports on interfacial bonding strength to provide an optimum annealing condition [26,28-31]. It is generally believed that bonding strength is a combined result of strengthening effect of atomic bonding and detrimental role of brittle IMC layer formed due to diffusion occurred during annealing process. It is noted here that the maximum bonding strength in the present Mg/Al two-ply clad sheet is achieved in A1 specimen annealed for 10 min at 300 °C, consistent with the previous reports [26,27]. The measured thickness of diffusion layers and average bonding strength are listed in Table 1.

3.3. Tensile test

True stress-strain curves given in Figs. 6(a) and (b) were obtained from tensile tests of monolithic constituent alloys

Table 1. Measured tensile properties of constituent alloys and Mg/Al clad sheet before and after annealing treatments

Materials	Mechanical Properties	Annealing Time (min)			
		0	10	30	60
AZ31 Mg Alloy	YS (MPa)	203.3	169.5	164.2	166.1
	UTS (MPa)	315.2	311.9	322.9	319.9
	UE (%)	13.0	16.5	17.2	17.1
	TE (%)	13.5	17.8	17.6	17.9
1050 Al Alloy	YS (MPa)	74.0	66.8	63.2	61.1
	UTS (MPa)	100.8	101.6	99.5	99.8
	UE (%)	11.0	16.5	15.5	17.2
	TE (%)	20.2	28.2	26.9	27.9
Mg/Al Clad Sheet	YS (MPa)	137.9	125.4	115.3	115.8
	UTS (MPa)	211.6	213.2	209.3	214.7
	UE (%)	12.7	16.1	16.6	17.0
	Elongation up to Mg Fracture (%)	13.6	22.5	19.8	17.6
	Thickness of Diffusion Layer (μm)	-	2.6 ± 0.19	6.2 ± 0.67	10.1 ± 0.74
	Average Bonding Strength (N/mm)	9.17 ± 0.69	11.42 ± 0.84	9.04 ± 0.69	4.76 ± 0.95

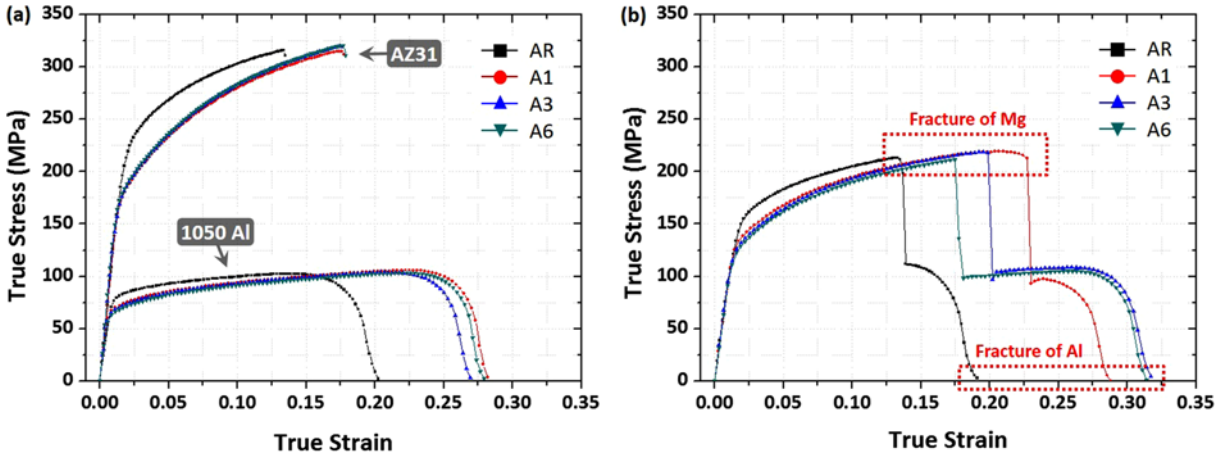

Fig. 6. True stress-strain curves of (a) monolithic constituent alloys and (b) two-ply Mg/Al clad sheet as a function of annealing time at 300 °C.

and Mg/Al two-ply clad sheets, respectively. The monolithic constituent alloys were separated from roll-bonded clad sheets (AR, A1, A3 and A6) by machining process. Monolithic AZ31 Mg and 1050 Al alloys taken from as-rolled AR sheet can be seen to have higher yield strength (YS) in Fig. 6(a) due to large strain-hardening during the roll-bonding process compared to annealed samples after roll-bonding. Both of the AZ31 Mg and 1050 Al alloys exhibited, however, large enhancement in elongation after annealing treatment with slight decrease in YS. Tensile properties of constituent alloys can be, on the other hand, observed not much different depending on annealing time from the figure. Two-ply clad sheets exhibited also a similar change in tensile properties due to annealing treatment compared to monolithic constituent alloys, except the strong dependence on annealing time as shown in Fig. 6(b). Two-stage fracture mode can clearly be observed to occur during the tensile test of clad sheets regardless of annealing condition from Fig. 6(b). The initial stress-drop observed in the figure was obviously caused by fracture initiation in the AZ31 Mg alloy side, which eventually leads into complete fracture of clad sheet in the second stage of fracture in the remaining 1050 Al alloy side. The largest elongation of 22.5% was obtained in A1 specimen before the fracture in AZ31 Mg alloy side, compared to the smallest elongation of 17.6% in A6 specimen. Tensile properties such as yield strength, ultimate tensile strength, and elongation are listed in Table 1.

3.4. Erichsen test

A series of Erichsen test has also been conducted for a monolithic 1050 Al alloy and AZ31 Mg alloy as well as two-ply Mg/Al clad sheet and the results are plotted as a function of annealing time in Fig. 7. The Erichsen values (IE) of this clad sheet were found much higher than those of monolithic AZ31 Mg alloy. The largest value was obtained after 10 min annealing with slightly decreasing trend with increasing annealing time after the peak value for the clad sheets. The cross-

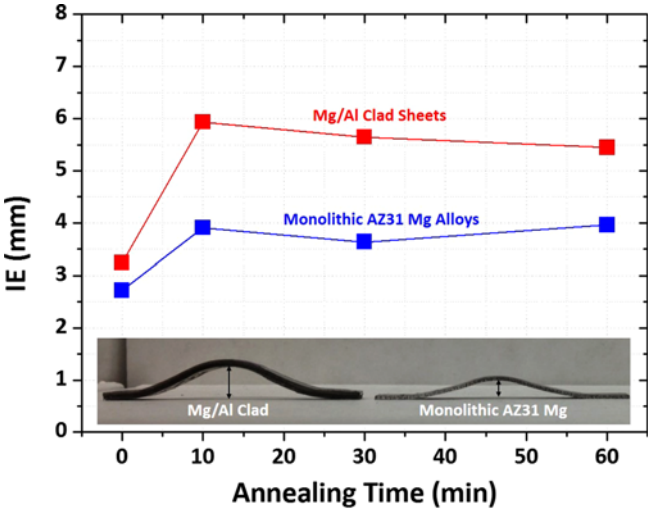

Fig. 7. Erichsen values of Mg/Al clad sheets are compared with those of monolithic AZ31 Mg alloys.

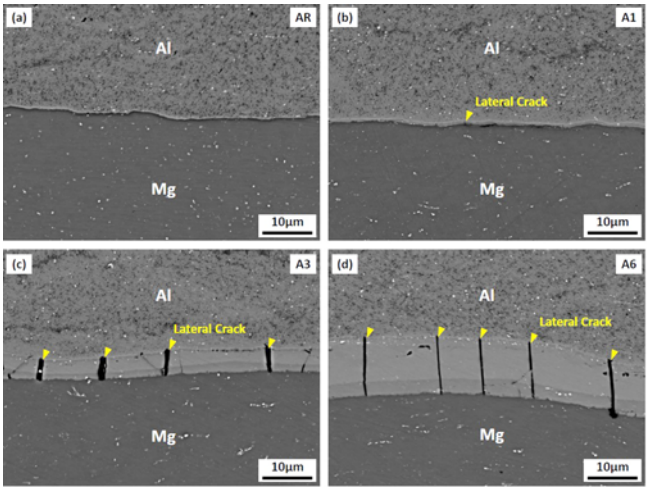

Fig. 8. Morphology change of Mg/Al interface after Erichsen test of (a) AR, (b) A1, (c) A3, and (d) A6 specimens.

sectional SEM image of Mg/Al interface of clad sheets after Erichsen test are given in Figs. 8(a) through (d), in which several cracks formed in the direction perpendicular to the layer seem to be arrested within the IMC layers in annealed samples. These cracks did not, however, propagate along the Mg/Al interface during the forming process.

4. DISCUSSION

Various tensile properties such as yield strength, ultimate tensile strength, and uniform elongation of clad sheets were estimated through the use of general rule of mixture and the results are plotted in Fig. 9 together with the experimentally measured values. The strength of two-ply laminate composite can be expressed as [32],

$$\sigma = A_{Mg}\sigma_{Mg} + A_{Al}\sigma_{Al} \quad (1)$$

with A and σ denoting the area and stress, respectively. Assuming the thickness of each constituent alloy is homogeneous along the unidirectional tensile direction, the fraction A can be substituted by the thickness of each constituent alloy. We can therefore easily predict both the YS and UTS values of two-ply clad sheets by using Eq. (1) to compare them with experimental values, as shown in Fig. 9(a). The elongation of two-ply clad materials is generally estimated by using the force based rule of mixture (ROM) [32-34]. The uniform elongation of two-ply laminate composite can then be expressed as,

$$\varepsilon_{clad}(u) = (A_{Mg}\sigma_{Mg}\varepsilon_{Mg}(u) + A_{Al}\sigma_{Al}\varepsilon_{Al}(u))/(A_{Mg}\sigma_{Mg} + A_{Al}\sigma_{Al}) \quad (2)$$

with ε(u) denoting uniform elongation of constituent alloys and clad plate. The uniform elongation of the present Mg/Al laminate composites is consequently estimated by using Eq. (2) to compare with experimental values, as given in Fig. 9(b).

These estimated values of tensile properties appear to match well with the experimental values for the present Mg/Al two-ply clad sheet regardless of annealing treatment condition, as can be clearly seen from the figures. This result alone cannot, however, provide a comprehensive understanding for characteristic mechanical behaviour of Mg/Al clad sheet, which exhibits somewhat different characteristics due to the existence of brittle IMC layers in Mg/Al interface compared to other clad materials studied so far [26,27,33,35-38]. These IMC layers consisted of $Mg_{17}Al_{12}$ and Mg_2Al_3 phases were formed and grew inevitably during the post heat treatment after roll-bonding process. The effects of this IMC layer on mechanical properties should be studied carefully for a more comprehensive understanding. Another important observation is that fracture strain of Mg alloy in Mg/Al clad sheet is much higher than that of monolithic Mg alloy, as shown in Fig. 9(b).

It has been reported that more ductile materials can effectively retard the formation of necking compared to less ductile materials to provide much improved overall total elongation for clad materials [32,35-37,39-43]. Enhanced fracture strain in the present Mg/Al clad sheets cannot, however, be accounted for by this difference in elongation, since they both have similar level of uniform elongation. The large enhancement of elongation in clad sheets can be explained due to the difference in post-necking behaviour of the two constituent alloys. Despite of similar tensile properties of constituent alloys, Mg/Al clad sheet exhibited large difference in fracture strain of Mg alloy depending on IMC layer growth, which in turn depended on annealing condition as observed in Fig. 9(b).

Digital image correlation analysis has consequently been conducted to elucidate further the effect of Mg/Al interfacial bonding strength on tensile properties of Mg/Al clad sheets. Strain distributions along the thickness direction were obtained during tensile tests for the four different clad sheets and the results are given in Figs. 10(a) through (d) to reveal thickness strain developed during the tests together with the uniform elongation ε_u denoted by black arrow lines. A larger thickness reduction of ~7.2% (blue coloured region) in Al ply can be

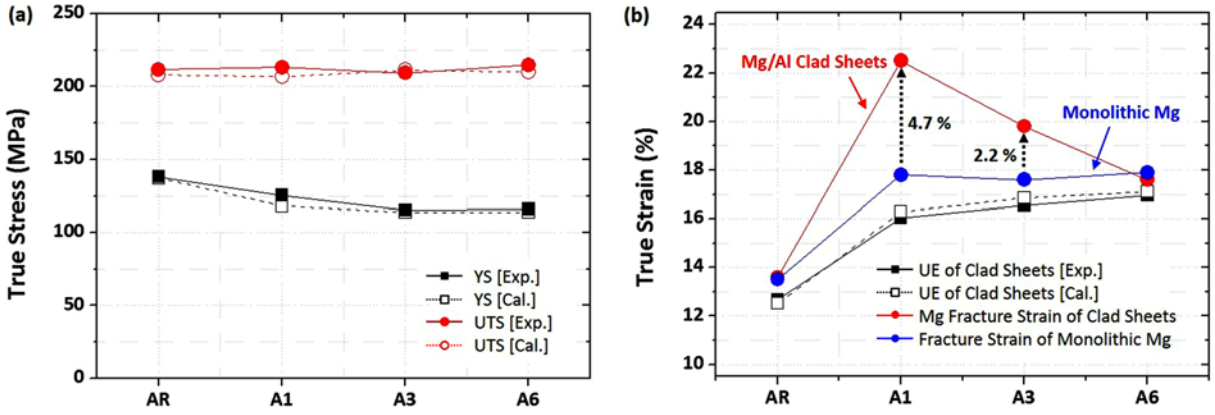

Fig. 9. Tensile properties of Mg/Al clad sheets are estimated by using a rule of mixture to compare with the experimental result: (a) yield strength and ultimate tensile strength and (b) uniform elongation and fracture strain.

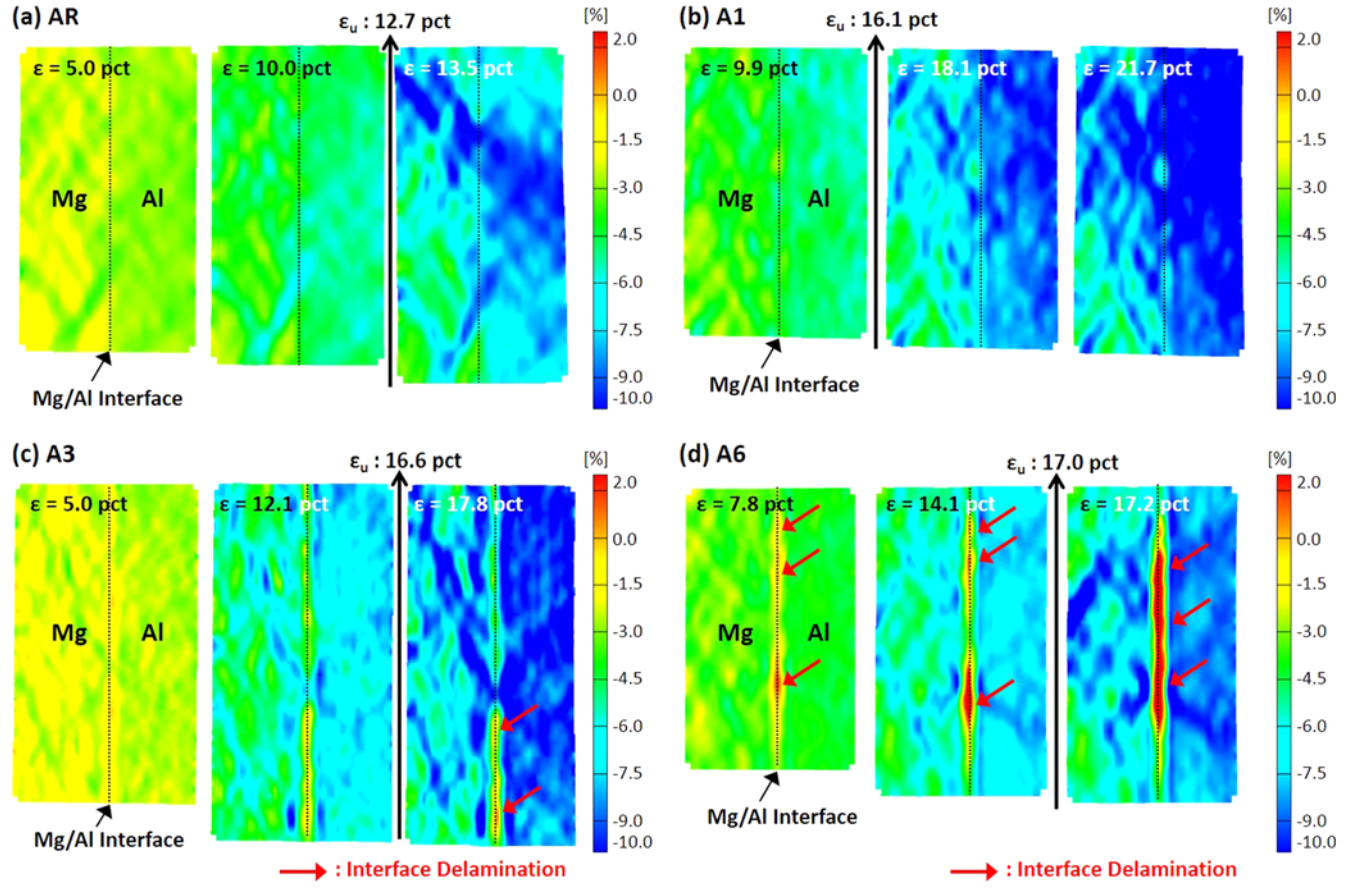

Fig. 10. Strain distribution along the thickness direction in (a) AR, (b) A1, (c) A3, and (d) A6 specimens.

observed from the figure compared to that of ~ 4.0% (green coloured region) in Mg alloy side. Negative strains can be seen to develop throughout in AR and A1 clad sheets from Figs. 10(a) and (b). On the other hand, somewhat different strain distributions are observed in A3 and A6 specimens. Non-uniform strain distribution was observed to develop in the Mg/Al interface of A3 specimen after 12.1% strain, represented by yellow coloured region in Fig. 10(c). Positive strain was even found to develop locally in the Mg/Al interface of A3 specimen at the strain of 17.8%, represented by red coloured region in Fig. 10(c), which in turn implies delamination of Mg/Al interface. This interface delamination was observed to develop locally at the much earlier strain of 7.8%, leading into complete interface delamination at 17.2% strain in A6 specimen. It can be concluded from the above results that the thickness of IMC layer should be limited less than 2.6 μm for a sound Mg/Al interface.

Interfacial bonding strengths were measured as 9.17 N/mm and 9.04 N/mm from the peel tests of AR and A3 clad sheets, respectively. Interfacial delamination was, however, observed after uniform elongation only in A3 clad sheets, despite of their similar bonding strengths. The bonding strength measured from the peel tests alone may not be properly related to tensile bonding strength. The thickness growth of IMC layer as shown in Fig. 5(a) appears therefore to influence the bonding strength, since these IMC layers could be under a more complex stress state during the tensile tests [26,35,38].

Changes in equivalent strain distribution during tensile tests are given in Figs. 11(a) through (d) to elucidate the effects of interfacial bonding strength on tensile behaviour of the four different clad sheets. Rapid localized necking can be observed in AR specimen due to large strain build up in Mg and Al alloy sides after uniform elongation, since AR specimen did not recover from heavy deformation accumulated during the prior roll-bond process. The clad sheets after various annealing treatment revealed large difference in deformation behaviour depending on the interfacial bonding strength, which was in turn influenced by the thickness of IMC layer. A1 specimen, for example, exhibited the best interfacial bonding strength leading into diffuse necking with homogeneous strain distribution both in Mg and Al alloy sides even after uniform elongation. Some localized regions of strain concentration were, however, observed to develop in the Mg/Al interface in A3 specimen, although the strain distributions in Mg and Al alloy were uniform during uniform elongation as can be seen from Fig. 11(c). These regions of strain concentration became much

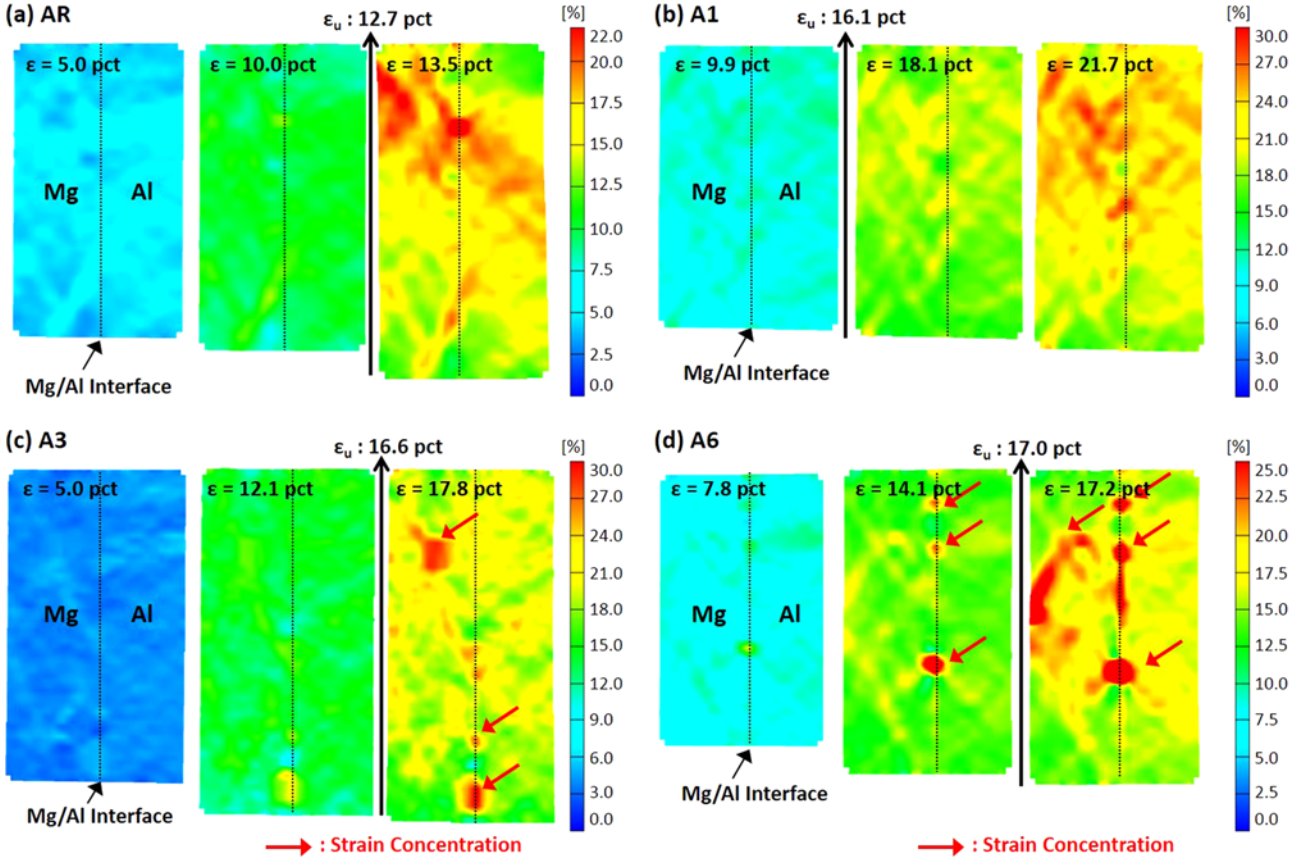

Fig. 11. Distribution of equivalent strain in (a) AR, (b) A1, (c) A3, and (d) A6 specimens.

larger after necking. At the larger strain of 17.8%, heavy strain concentration can also be observed in the Mg alloy side to cause localized necking, while Al alloy side still maintained relatively uniform strain distribution. This strain concentration in the Mg/Al interface in A6 specimen was found to develop much earlier at the strain of 14.1% together with non-uniform strain distribution both in the Mg and Al alloy sides, as shown in Fig. 11(d). Complete interface delamination occurred at the strain of 17.2% with much larger strain concentration in the interface and Mg alloy side resulting into localized necking, which shows a good agreement with the tensile properties previously given in Figs. 6(b) and 9(b).

The fracture strain of Mg alloy in clad sheet was found to increase to 22.5% compared to 17.8% of monolithic AZ31 Mg alloy, 26% increase, when the IMC layer was limited below a certain thickness value as discussed before. This ductility enhancement in clad Mg alloy cannot be accounted for by conventional approach in terms of delayed necking. It is therefore necessary to clarify the difference in post-necking behaviour between AZ31 Mg and 1050 Al alloys. The post-necking behaviour of monolithic Mg alloy was seen from Fig. 6(a) to lead into fracture without diffuse necking, while monolithic Al alloy fractured after somewhat large strain of diffuse necking as listed in Table 1. The uniform elongations of monolithic Mg and Al alloys are not much different to provide very limited influence on each other in terms of postponing necking. The ductility enhancement in clad Mg alloy appears due to the diffuse necking behaviour of clad Al alloy. Complex triaxial stress state within necked region could also provide detrimental effects on tensile properties of Mg/Al two-ply clad sheets, due to the existence of brittle IMC layer. A similar result has recently been reported by Jin *et al.* [44], in which enhanced ductility of Al/STS clad sheet was attributed to suppression of localized neck and enhancement of homogeneous deformation due to mutual constraint imposed by adjacent layers.

This ductility enhancement of clad Mg alloy, caused by delayed localized necking, could be observed more clearly from the results of Erichsen tests given in Fig. 7, where the ductility of clad Mg alloy was seen to increase much compared to those of monolithic Mg alloy. This ductility enhancement appears, therefore, due to more homogeneous deformation of clad Mg alloy when clad with Al alloy, which have appreciable diffuse necking region. EBSD results of A1 specimen given in Figs. 12(a) and (b) were obtained from the cross section of top region after the punch height reached 3.5 mm during the Erichsen test. Large number of shear bands can be observed to form within the grains of Mg alloy during the tests, evidenced by an inverse pole figure (IPF) and kernel average

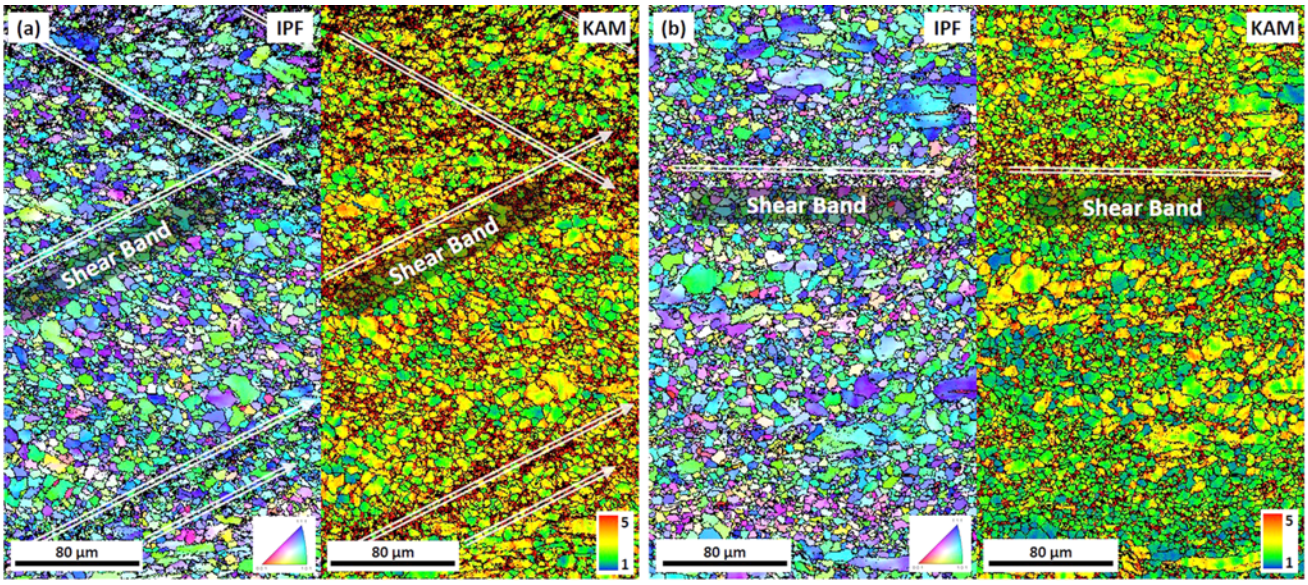

Fig. 12. Inverse pole figure (IPF) and kernel average mis-orientation (KAM) maps of AZ31 Mg alloys after annealing for 10 min at the same punch height of 3.5 mm: (a) monolithic, and (b) clad AZ31 Mg alloy sheet.

misorientaion (KAM) map of monolithic Mg alloy given in Fig. 12(a). Here, the KAM was calculated up to the fifth neighbor shell with a maximum misorientation angle of 5°. These shear band formation is well known to reduce room temperature formability of Mg alloys [45-47]. Clad Mg alloy with Al exhibits, on the other hand, very limited number of shear bands with relatively homogeneous deformation, as can be seen from Fig. 12(b). Cladding Al alloy to Mg alloy appears to induce more homogeneous deformation to inhibit shear band formation resulting into ductility enhancement of Mg alloy.

Another noteworthy result of Erichsen tests was that annealing time did not affect the formability of clad sheets, contrary to tensile test results, as shown in Fig. 7. This difference between tensile test and Erichsen tests is thought due to different crack propagation behaviour due to IMC layer during the tests. The interface microstructures after Erichsen tests given in Fig. 8 exhibited relatively sound Mg/Al interface in AR and A1 specimens, while a few cracks were observed to generate in A3 and A6 specimens. Delamination did not occur in AR and A1 specimens during the tensile tests, contrary to A3 and A6 specimens exhibiting a local and complete interface delamination. Cracks were, however, also observed to form in perpendicular direction to interface within the IMC layer of A3 and A6 clad sheets, but propagated along the interface to prevent interface delamination maintaining interfacial bonding between Mg and Al alloys during Erichsen tests. This lateral crack propagation behaviour within the IMC layer prevented interface delamination in A3 and A6 specimens resulting into ductility enhancement of clad Mg alloy regardless annealing times of clad sheets during Erichsen tests.

5. CONCLUSIONS

Two-ply Mg/Al clad sheets were first fabricated by a roll-bonding process followed by annealing treatments. Their interfacial bonding properties were then investigated in relation to deformation behavior under tensile test and Erichsen test.

(1) The Mg/Al interface in as-roll-bonded and annealed samples is clearly observed not to contain any pores, cracks, or lateral delamination. The composition profiles in the Mg/Al interface provided a clear evidence for atomic diffusion occurred during an annealing treatment at 300 °C, to form brittle IMC layers identified as $Mg_{17}Al_{12}$ and Mg_2Al_3 phases from the Al-Mg phase diagram. The thickness of IMC layers was found to increase by extending annealing time. Average bonding strength increased up to annealing time of 10 min, but then decreased with increasing time after the peak strength.

(2) After annealing treatments at 300 °C, AZ31 Mg and 1050 Al alloys were observed to have similar tensile properties regardless of annealing time. However, the Mg/Al clad sheets after various annealing treatment revealed large difference in deformation behaviour depending on interfacial bonding strength, which was in turn influenced by the thickness of IMC layer. A1 specimen exhibited the best interfacial bonding strength leading into diffuse necking with homogeneous strain distribution both in Mg and Al alloy sides even after uniform elongation.

(3) Present Mg/Al two-ply clad sheet provided much higher Erichsen value (IE) compared to those of monolithic AZ31 Mg alloy. This ductility enhancement appears due to more homogeneous deformation of clad Mg alloy, inhibiting formation of shear band. Lateral cracks were formed in perpen-

dicular direction to interface within the IMC layer of annealed clad sheets, but propagated along the interface to prevent interface delamination maintaining interfacial bonding, resulting into ductility enhancement of clad Mg alloy regardless annealing times for clad sheets during Erichsen tests.

ACKNOWLEDGMENTS

This study was supported by Brain Korea 21 PLUC Project for Center for Creative Industrial Materials, the Fundamental R&D Program for Core Technology of Materials of the Ministry of Knowledge Economy, Korea, under the contract No. 10037273 and also by POSCO under the contract No. 2014Y008.

REFERENCES

1. B. A. Movchan and F. D. Lemkey, *Mater. Sci. Eng. A* **224**, 136 (1997).
2. G. Heness, R. Wuhrer, and W. Y. Yeung, *Mater. Sci. Eng.* **483**, 740 (2008).
3. S. E. Lee, K. S. Lee, M. J. Kim, and Y. N. Kwon, *Korean J. Met .Mater.* **52**, 605 (2014).
4. S.-T. Hong, K. S. Weil, I.-T. Bae, J. P. Choi, and J. Pan, *J. Power Sources* **195**, 2592 (2010).
5. Y. M. Jo, K. S. Lee, N. Kang, and Y.-S. Lee, *Korean J. Met. Mater.* **52**, 881 (2014).
6. J. E. Lee, D. H. Bae, W. S. Chung, K. H. Kim, J. H. Lee, and Y. R. Cho, *J. Mater. Process. Technol.* **185**, 546 (2007).
7. J. C. Benedyk, *Light Met. Age* **63**, 36 (2005).
8. K. Westphal, T. Mulherkar, and W. Scheiding, *Light Met. Age* **63**, 42 (2005).
9. A. A. Wang, S. Sircar, and J. Mazumder, *J. Mater. Sci.* **28**, 5113 (1993).
10. B. L. Mordike and T. Ebert, *Mater. Sci. Eng. A* **302**, 37 (2001).
11. A. Srinivasan, U. T. S. Pillai, and B. C. Pai, *Metall. Mater. Trans. A* **36**, 2235 (2005).
12. E. P. Banczek, L. M. C. Zarpelon, R. N. Faria, and I. Costa, *J. Alloys Compd.* **479**, 342 (2009).
13. N. Bay, *Met. Constr.* **18**, 486 (1986).
14. P. P. Gudur, M. A. Salunkhe, and U. S. Dixit, *Int. J. Mech. Sci.* **50**, 315 (2008).
15. L. Li, K. Nagai, and F. Yin, *Sci. Technol. Adv. Mater.* **9**, 1 (2008).
16. A. Çetin, J. Krebs, A. Durussel, A. Rossoll, J. Inoue, T. Koseki, S. Nambu, and A. Mortensen, *Metall. Mater. Trans. A* **42**, 3509 (2011).
17. X. P. Zhang, M. J. Tan, T. H. Yang, X. J. Xu, and J.T. Wang, *Bull. Mater. Sci.* **34**, 805 (2011).
18. X. Li, G. Zu, M. Ding, Y. Mu, and P. Wang, *Mater. Sci. Eng.* A **529**, 485 (2011).
19. G. Shi and J. Qiao, *Adv. Mat. Res.* **239**, 50 (2011).
20. Y. Wang, S. B. Kang, and J. Cho, *J. Alloys Compd.* **509**, 704 (2011).
21. *ASTM E 8/E 8M Annual Book of ASTM Standards* (ASTM, 2007).
22. *ASTM-D3167 Annual Book of ASTM Standards* (ASTM, 2007).
23. J. H. Bae, A. K. Prasada Rao, K. H. Kim, and N. J. Kim, *Scr. Mater.* **64**, 836 (2011).
24. M. C. Chen, C. C. Hsieh, and W. Wu, *Met. Mater. Int.* **13**, 201 (2007).
25. N. Saunders, *Calphad* **14**, 61 (1990).
26. K. S. Lee, J. -S. Kim, Y. M. Jo, S. E. Lee, J. Heo, Y. W. Chang, and Y. S. Lee, *Mater. Charact.* **75**, 138 (2013).
27. J.-S. Kim, K. S. Lee, Y. N. Kwon, B.-J. Lee, Y. W. Chang, and S. Lee, *Mater. Sci. Eng.* A **628**, 1 (2015).
28. H.-Y. Wu, S. Lee, and J.-Y. Wang, *J. Mater. Process. Technol.* **75**, 173 (1998).
29. L. M. Liu, X. J. Liu, and S. Liu, *Scr. Mater.* **55**, 383 (2006).
30. L. M. Liu, J. H. Tan, L. M. Zhao, and X.J. Liu, *Mater. Charact.* **59**, 479 (2008).
31. C. F. Liu, J. Zhang, Y. Zhou, H. L. Yi, and M. Naka, *J. Alloys Compd.* **471**, 217 (2009).
32. S. L. Semiatin and H. R. Piehler, *Metall. Trans. A* **10**, 85 (1979).
33. D. R. Lesuer, C. K. Syn, O. D. Sherby, J. Wadsworth, J. J. Lewandowski, and W. H. Hunt, *Int. Mater. Rev.* **41**, 169 (1996).
34. S.-H. Choi, K.-H. Kim, K. H. Oh, and D. N. Lee, *Mater. Sci. Eng.*A **222**, 158 (1997).
35. J. Inoue, S. Nambu, Y. Ishimoto, and T. Koseki, *Scr. Mater.* **59**, 1055 (2008).
36. S. Nambu, M. Michiuchi, J. Inoue, and T. Koseki, *Compos. Sci. Technol.* **69**, 1936 (2009).
37. S. Nambu, M. Michiuchi, Y. Ishimoto, K. Asakura, J. Inoue, and T. Koseki, *Scr. Mater.* **60**, 221 (2009).
38. K. S. Lee, D. H. Yoon, H. K. Kim, Y. -N. Kwon, and Y.-S. Lee, *Mater. Sci. Eng.* A **556**, 319 (2012).
39. N. Yamamoto, J. Liao, S. Watanabe, and K. Nakata, *Mater. Trans.* **50**, 2833 (2009).
40. D. Embury and O. Bouaziz, *Annu. Rev. Mater. Res.* **40**, 213 (2010).
41. E. W. Jeong, K. N. Hui, D.-H. Bae, D. S. Bae, and Y.-R. Cho, *Met. Mater. Int.* **20**, 499 (2014).
42. I. K. Kim and S. I. Hong, *Metall. Mater. Tran. A* **44**, 3890 (2013).
43. W. N. Kim and S. I. Hong, *Mater. Sci. Eng. A* **651**, 976 (2016).
44. J. Y. Jin and S. I. Hong, *Mater. Sci. Eng. A* **596**, 1 (2014).
45. M. R. Barnett, M. D. Nave, and C. J. Bettles, *Mater. Sci. Eng. A* **386**, 205 (2004).
46. Y. Chino, K. Sassa, A. Kamiya, and M. Mabuchi, *Mater. Sci. Eng. A* **441**, 349 (2006).
47. Y. Chino, M. Kado, and M. Mabuchi, *Mater. Sci. Eng. A* **494**, 343 (2008).